JOURNAL OF MAGNETIC RESONANCE **131,** 177–183 (1998)
ARTICLE NO. MN981366

# Control of Spinning Sidebands in High Resolution NMR Spectroscopy

M. W. Borer and S. R. Maple[1]

*Eli Lilly and Company, Lilly Research Laboratories, Indianapolis, Indiana 46286*
E-mail: MAPLE_STEVEN_R@Lilly.com

Received July 18, 1997; revised October 6, 1997

**The presence of spinning sidebands can severely compromise the detection of low molarity analytes. Spinning sidebands have traditionally been minimized by improving the magnetic field homogeneity and by varying the spinning of the sample in a linear fashion during data acquisition. The effect of the latter is to spread the spinning sideband intensity over a range of frequencies so that the final result is a spinning sideband whose shape reflects the distribution of spinning speeds. We have designed a customized profile of spinner speed variation that optimizes the reduction of spinning sidebands. The customized profile is based on theoretical considerations of how the intensity of sidebands vary with the rate of sample rotation and also compensates for the mechanical design of the spinner mechanism. The result is a unique combination of an exponential increase in gas flow rate to balance the theoretical considerations coupled with a strategically placed rapid change in air flow to annul the sluggish response of the spinning mechanism to acceleration. The resulting sideband shape is a broad, flat, square step in the baseline that is least likely to interfere with low molarity analyte peaks.** 

## INTRODUCTION

The use of NMR spectroscopy in the detection of low-molarity analytes is well documented. Many papers have dealt with the important issue of dynamic range and methods for overcoming this problem via solvent suppression using techniques such as shifted-laminar-pulses (*1*), WATERGATE (*2*), and more recently the WET family of pulse sequences (*3, 4*). Our desire is to observe low-molarity analytes without using solvent suppression techniques. The motivation for doing this is to observe signals from low-molarity analytes, $\leq$0.05% of the largest component, very close to signals from the major components, and to use the $^{13}$C satellites observed in the proton spectrum as intensity references. In order to do this there must not be the possibility of intensity perturbation, the lineshapes must be of high quality, and spurious signals, especially spinning sidebands, must be controlled. Since solvent suppression will not be used, the first criterion is satisfied. Modern NMR spectrometers, appropriately configured, have the ability to achieve and maintain high quality lineshapes given the current state of probe and shim system design and implementation. The control of spinning sidebands is the subject of this article.

[1] To whom correspondence should be addressed. Fax: (317) 277-8387.

## THEORY

The theory of spinning sidebands has been described by Williams and Gutowsky (*5*), Dadok (*6*), and Allerhand and Maple (*7*). As originally developed by Williams and Gutowsky the theory of spinning sidebands assumed, quite correctly at that time, that spinning sidebands were due primarily to samples spinning in the presence of linear $H_0$ gradients perpendicular to the axis of rotation. Under these conditions, spinning sidebands are observed whose relative integrated intensities are given by

$$A_{\pm n}(k) = J_n^2(k) - J_{n-1}(k)J_{n+1}(k), \quad [1]$$

where $k$, the modulation index, is defined by

$$k = \gamma H_1^{00}/2\pi\nu_s, \quad [2]$$

where $\nu_s$ is the spinning speed and $J_n$ is the Bessel function of order $n$ for the argument $k$. When $k \ll 1$, Bessel functions simplify to

$$J_n(k) = (k/2)^n/n!. \quad [3]$$

Substituting Eq. [3] into Eq. [1] yields

$$A_{\pm n}(k) = (k/2)^{2n}/n!(n+1)!. \quad [4]$$

The ratio of integrated intensities for two adjacent spinning sidebands using Eq. [4] is given by

$$A_{\pm(n+1)}(k)/A_{\pm n}(k) = (k/2)^2/(n+1)(n+2). \quad [5]$$



1090-7807/98 $25.00

The theory of Williams and Gutowsky also predicts the behavior of spinning sidebands as the spinning speed increases. From Eq. [4] it follows that the ratio of integrated intensities for two values of the modulation index, $k$ and $k'$, is given by

$$A_{\pm n}(k)/A_{\pm n}(k') = (k/k')^{2n} = (\nu_s'/\nu_s)^{2n}. \qquad [6]$$

Consider the implications of Eqs. [5] and [6] to the intensity and appearance of spinning sidebands. For a linear field gradient of 4 Hz and a spinning speed of 20 Hz, $k = 0.2$. Equation [4] predicts that $A_{\pm 1}$ and $A_{\pm 2}$ should be 0.5 and 0.0008%, respectively, clearly indicating that only first-order spinning sidebands should be observed. Equation [6] predicts that $A_{\pm 1}$ should decrease from 0.5% ($k = 0.2$) to 0.33% as $\nu_s$ increases from 20 to 30 Hz.

Traditional methods for minimizing the intensity of spinning sidebands have involved varying the spinning speed in a linear fashion to distribute the spinning sideband intensity over a range of spinning speeds (*8*). From the standpoint of detection of low molarity analytes, the spinning sideband peak height, $P_n$, is more important than the integrated intensity, $A_n$. Under a linear variation of $\nu_s$ between a lower limit of $\nu_s^L$ and upper limit $\nu_s^U$, each spinning sideband will undergo a broadening of $|n|(\nu_s^U - \nu_s^L)$, and a resulting decrease in $P_n$. The ratio of $P_n$ at a fixed $\nu_s$ and in the presence of spinner speed variation between $\nu_s^L$ and $\nu_s^U$ is approximately

$$P_n^F/P_n^V = W_{ex}^{-1}[W_{ex} + |n|(\nu_s^U - \nu_s^L)],$$

where $P_n^F$ and $P_n^V$ are the values of $P_n$ at a fixed $\nu_s$ and in the presence of spinner speed variation, respectively, and $W_{ex}$ is the linewidth at half-height for fixed $\nu_s$. The practical limit on values of $(\nu_s^U - \nu_s^L)$ which maintain high resolution and stability is about 10 Hz. Therefore, the upper limit to the reduction of $P_n^F$ by spinner speed variation for $W_{ex} = 1.0$ Hz, a typical value for proton linewidths, is about a factor of $10|n|$. Given this constraint it is important to optimize the manner in which the spinner speed variation is implemented.

The previous theoretical discussion on the formation of spinning sidebands focused on samples spinning through linear $H_0$ gradients perpendicular to the axis of rotation. In the absence of $H_0$ gradients, or when $H_0$ gradients are minimized, other mechanisms exist for the formation of spinning sidebands (*6, 7*). Dadok has described in some detail these mechanisms which involve $H_1$ inhomogeneity and variable coupling of the precessing magnetization to the receiver coil (*6*). On our spectrometer, the overwhelming mechanism for spinning sidebands are $H_0$ gradients perpendicular to the axis of rotation. This conclusion is supported by several observations. Only first-order spinning sidebands are visible in spectra acquired with optimal $H_0$ homogeneity ($P_{\pm 1} \leq 0.1\%$). A substantial degradation of $H_0$ homogeneity is required before second-order sidebands become visible, but higher order sidebands have not been observed. Table 1 shows the $P_{\pm 1}$ and $A_{\pm 1}$ for spinning sidebands recorded at various spinning speeds and a comparison of the integrated intensity for a given spinning sideband at $\nu_s$ and the corresponding sideband at $\nu_{s+5}$. Examination of these $P_{\pm 1}$ and $A_{\pm 1}$ values indicates that under the conditions described in Table 1 the observed spinning sidebands follow the theory of Williams and Gutowsky as detailed in Eqs. [4]–[6].

**TABLE 1**[a]

| $\nu_s$ (Hz) | $n$ | $P_{\pm n}$ | $A_{+n}$ | $A_{+n}(\nu_s)/A_{\pm n}(\nu_s + 5)$[b] |
|---|---|---|---|---|
| 15 | +1 | 0.99 | 1.1 | 1.9 (1.8) |
| 15 | −1 | 0.92 | 1.0 | 1.5 (1.8) |
| 20 | +1 | 0.50 | 0.57 | 1.3 (1.6) |
| 20 | −1 | 0.60 | 0.68 | 1.9 (1.6) |
| 25 | +1 | 0.43 | 0.45 | 1.1 (1.4) |
| 25 | −1 | 0.38 | 0.36 | 1.2 (1.4) |
| 30 | +1 | 0.25 | 0.41 | |
| 30 | −1 | 0.28 | 0.29 | |

[a] The spinning sideband peak height ($P$) and integrated amplitude ($A$) are expressed as a percentage of the centerband.

[b] The values tabulated here are acutal (expected) as derived from either Eq. [4] or [5].

## RESULTS AND DISCUSSION

In order to explore the effect of variation in spinner speed we chose as a test sample the indirect detection calibration sample, $^{13}$C-enriched methyl iodide. Figure 1 shows the $\pm 120$ Hz region of the proton spectrum of $CH_3I$. The central line of the pseudo-triplet in the bottom spectrum of Fig. 1 arises from $^{12}CH_3I$ and the outer two lines arise from $^{13}CH_3I$. The peaks marked with asterisks are first-order spinning sidebands with $P_{\pm 1} = 3.5\%$. This level of spinning sidebands was induced by misadjusting the X-gradient shim and allowed the behavior of the spinning sidebands to be readily observed. It is important to note that only first-order spinning sidebands are visible.

A key factor discovered during initial experiments was that the spinner in this instrument, and undoubtedly in spinner assemblies for other commercial instruments, does not respond quickly to changes in spinner air flow. The response is especially sluggish when the spinner must change from decelerating to accelerating. Presumably, this is because there is very little friction between the gas flow and the spinner, and the spinner has a corre-

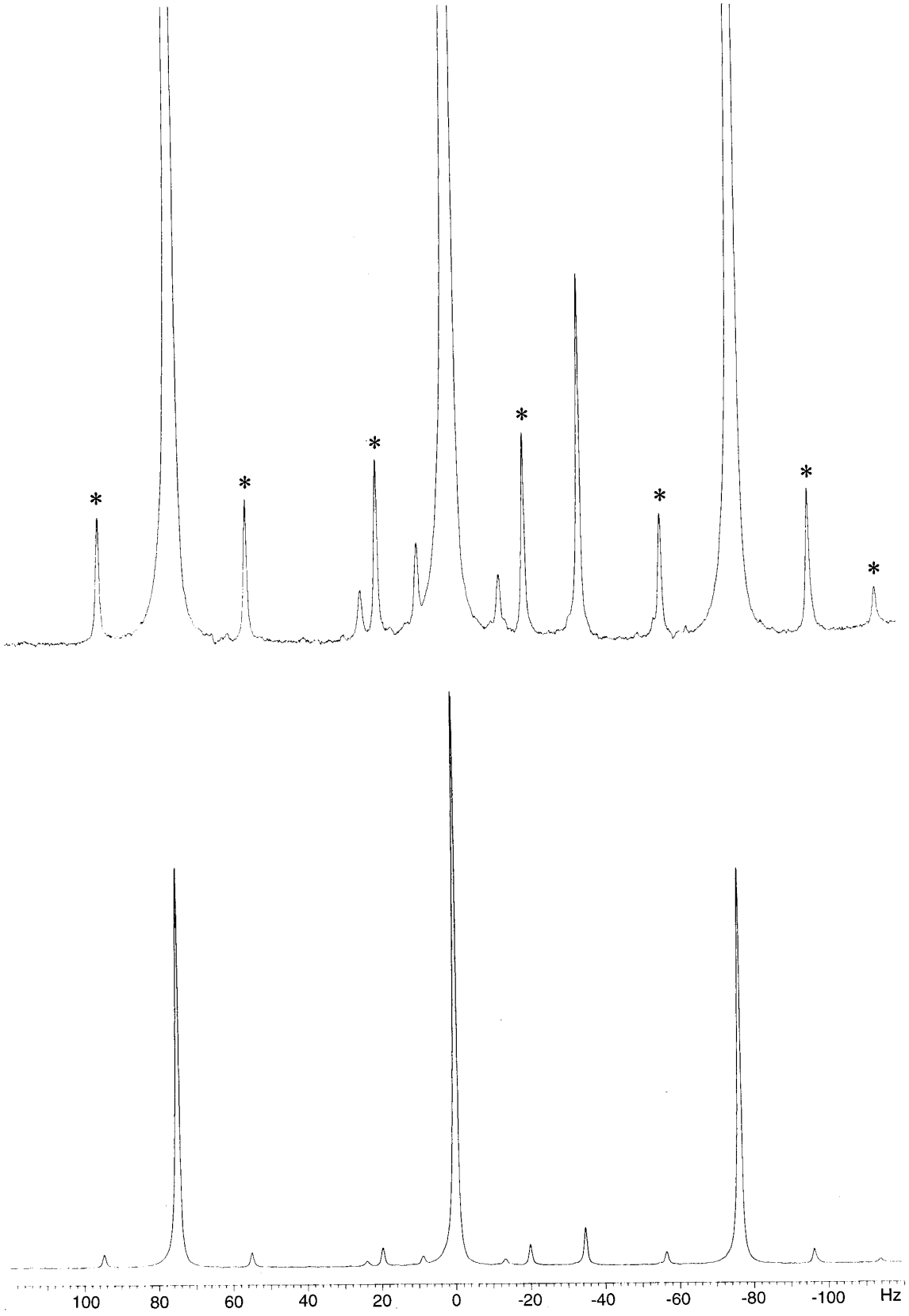


**FIG. 1.** The ±120 Hz region of the proton spectrum of $^{13}CH_3I$. The sample is an indirect detection calibration standard consisting of 1% $^{13}CH_3I$, 1% TMP, 0.2% $cr(acac)_3$, and 97.8% $CDCl_3$. The top spectrum is a 10-fold increase in the vertical scale of the bottom spectrum. Note that the rightmost labeled peak is a spinning sideband arising from a peak that is outside of the displayed range. The asterisks (*) identify first-order spinning sidebands.

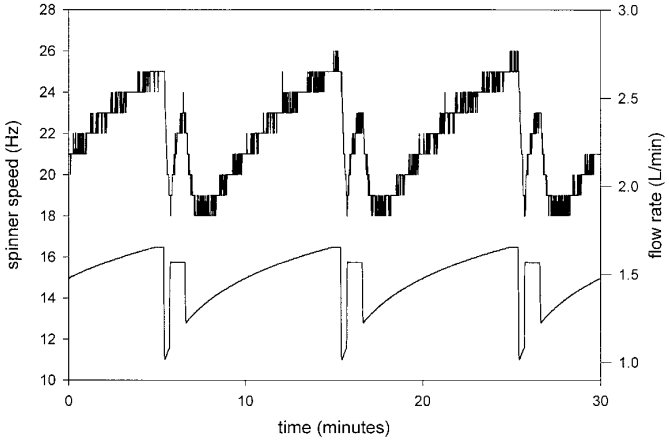


**FIG. 2.** The customized variation in air flow and the resulting time profile of spinning speed. The lower trace is the air flow reading from the mass flow meter and corresponds to the right *y* axis. The upper trace is the resulting variation in the sample spinning speed and corresponds to the left *y* axis.

spondingly high inertia. For the same reason, the rate of deceleration with a step decrease in flow rate was found to be greater than the rate of acceleration with a step increase in flow rate. These factors make it difficult to program a planned change in spinner speed with time. Specifically, a linear variation of $\nu_s$ would not result in an equal amount of time at each spinner speed. Rather, the sample would spend more time spinning at the slower spinner speeds leading to more intensity in the spinning sideband as $\nu_s$ approaches $\nu_s^L$. The quickest change in gas flow rate would have to be much slower than the slowest response time of the spinner so that the spinner speed always matches the flow. This turns out to be a very low frequency ($\ll$0.001 Hz), resulting in a very long acquisition time to complete one period of spinner speed variation. To completely distribute $P_n$ it becomes advantageous to collect data over more than one period of $\nu_s$ variation.

Another consideration that must be taken into account when choosing a spinner speed profile is the behavior of $P_n$ as a function of spinner speed as presented in Eq. [6]. The intensity of a given spinning sideband increases as $\nu_s$ becomes smaller. In order to uniformly spread out a given spinning sideband, it is necessary to design a spinner speed profile where more time is spent spinning at higher $\nu_s$ and less time at lower $\nu_s$. Unfortunately, the inertia of the spinner causes a long lag at low $\nu_s$ as the gas flow rate changes from decreasing to increasing. To effectively resolve this dilemma, and compensate both for spinner inertia and the behavior of spinning sidebands with respect to $\nu_s$, we designed a custom spinner speed profile. This waveform is displayed as the time function of gas flow rate in Fig. 2. The overall shape is an exponential increase that is intended to counterbalance the change in spinning sideband intensity with $\nu_s$. We have also added a pulse following the drop in flow at the beginning of the exponential increase. This pulse compensates for the lag at low $\nu_s$ caused by the spinner's inertia and actually causes the spinner speed to temporarily increase again. The temporal position, length of time, and intensity of the pulse have all been empirically optimized to counterbalance the lag. The resulting spinner speed profile, also in Fig. 2, is complex but results in the appropriate amount of time spent at each spinning speed for optimal shaped sidebands.

Figure 2 also shows the time scale over which this variation takes place. The period of one waveform is 10 min., several multiples of which is a reasonable data collection time for low molarity component detection. If the rate of change becomes too fast, the spinning speed profile cannot change fast enough to correlate to the changing air flow. For example, a period of 2 min. with the same air flow profile results in a distorted $\nu_s$ profile that does not have the desired effect on the sideband shape. It was also observed that as the period is increased, the characteristics of the pulse in air flow must be modified to maintain the same effect on the sideband shape. Note that the measured air flow rate exactly tracked the set point of the flow controller for the rate of change used in these experiments.

The $^{12}CH_3I$ resonance in Fig. 1 was used to demonstrate the effect of this customized variation of $\nu_s$. Figure 3 shows spectra collected from one scan (5.8 s) up to 416 scans (40 min.). The single scan is representative of fixed $\nu_s$ because $\nu_s$ does not change appreciably during 5.8 s. As the data collection time increases, the shape of the sideband approaches the average of the entire profile of $\nu_s$. At one or more full periods, the sideband shape becomes an even distribution of intensity across the spinning speed. These flat wide sidebands provide the best background against which to detect low molarity signal peaks. At more typical levels of spinning sidebands without the misadjusted X-gradient shim, this profile reduces the sidebands below the level of background noise.

Figure 4 displays the pseudo-triplet region with and without our customized variation in $\nu_s$ and with the X-gradient shim adjusted to the same level as in Figs. 1 and 3. Note that the four low-level component peaks marked by asterisks become more clearly defined as constituent peaks and cannot be mistaken for sideband signals. More importantly an additional trace component peak (marked with a †) that was completely obscured by a spinning sideband becomes visible with spinning speed modulation.

## CONCLUSION

The approach presented here is designed to facilitate the detection of very minor resonances in spectra with a high

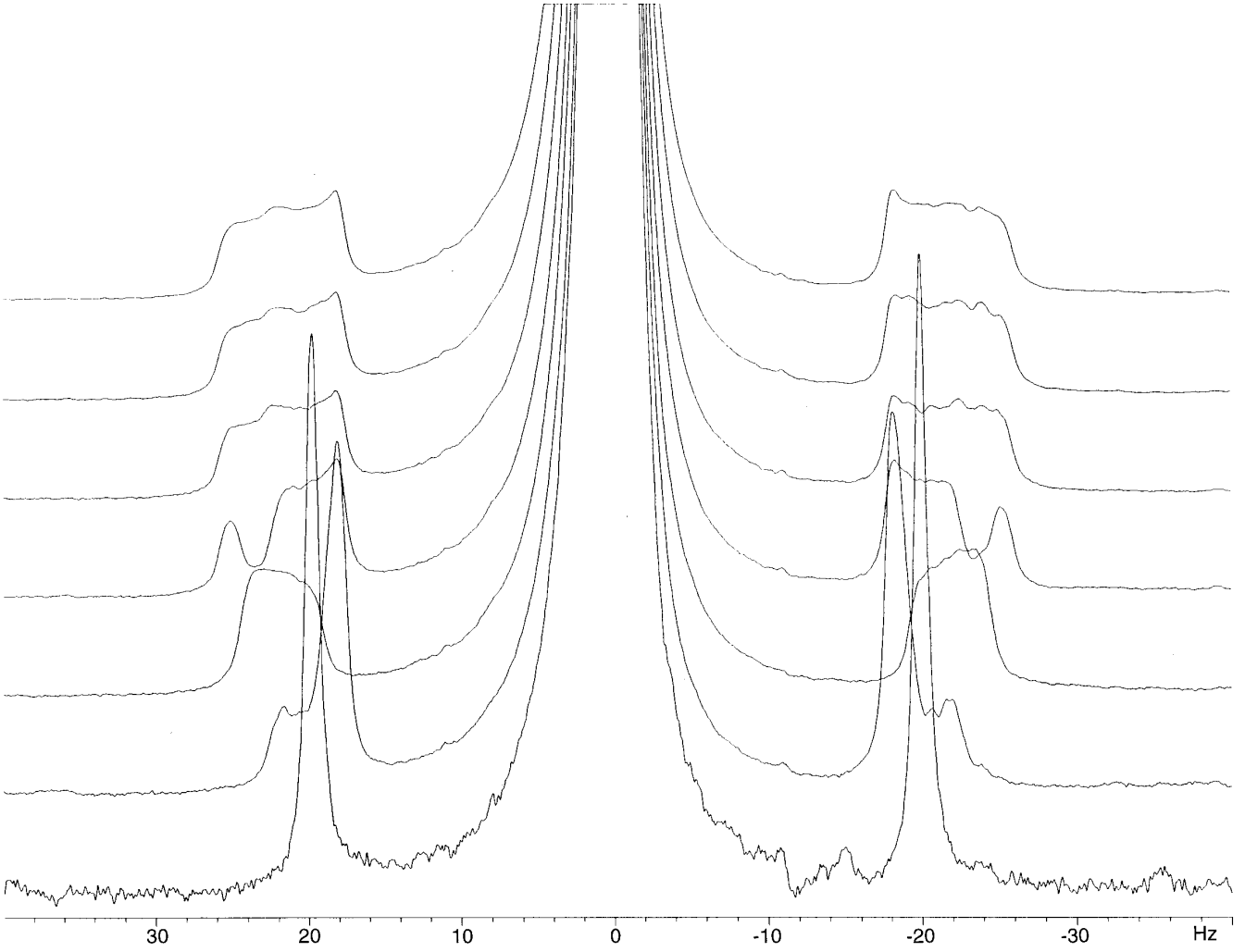


**FIG. 3.** Overlay of the $^{12}CH_3I$ resonance and corresponding spinning sidebands with increasing data collection time. The bottom trace corresponds to one scan or about 5.8 s. The next spectrum is the average of 26 scans corresponding to 25% of the 10-min. period of spinning speed variation. Subsequent spectra are 52, 78, 104, 208, and 416 scans corresponding to 50, 75, 100, 200, and 400% of the $\nu_s$ period.

dynamic range by minimizing the residual height of sinning sidebands and producing a residual spinning sideband shape which can be easily differentiated from ''real'' signals. Through the customized variation of spinning speed, an optimial reduction in spinning sidebands can be achieved. This variation profile accounts for theoretical differences in sideband intensity with spinning frequency and for the mechanical design of the spinning mechanism. This inexpensive simple approach virtually eliminates sidebands in modern high resolution NMR instruments. While the previous discussion has focused on a situation where the main contribution to spinning sidebands is $H_0$ inhomogeneity, the application of a customized variation in the sample spinning speed can effectively minimize spinning sidebands arising from other mechanisms.

## EXPERIMENTAL

To determine the optimum spinner speed variation profile, the flow of spinner air was regulated with a model FMA-469-V mass flow controller from Omega Instruments. The set point of the controller was automatically varied with an analog output from a National Instruments NB-MIO-16XL-18 interface card and National Instruments LabVIEW 2.1 software. The LabVIEW program was run on an Apple Macintosh IIci. A custom virtual instrument (VI) was designed to output the desired spinner speed profile to the mass flow controller.[2] The shape, frequency, zero offset, and amplitude of the profile are all user programmable. A second custom

[2] The custom VI is available from the authors upon request.

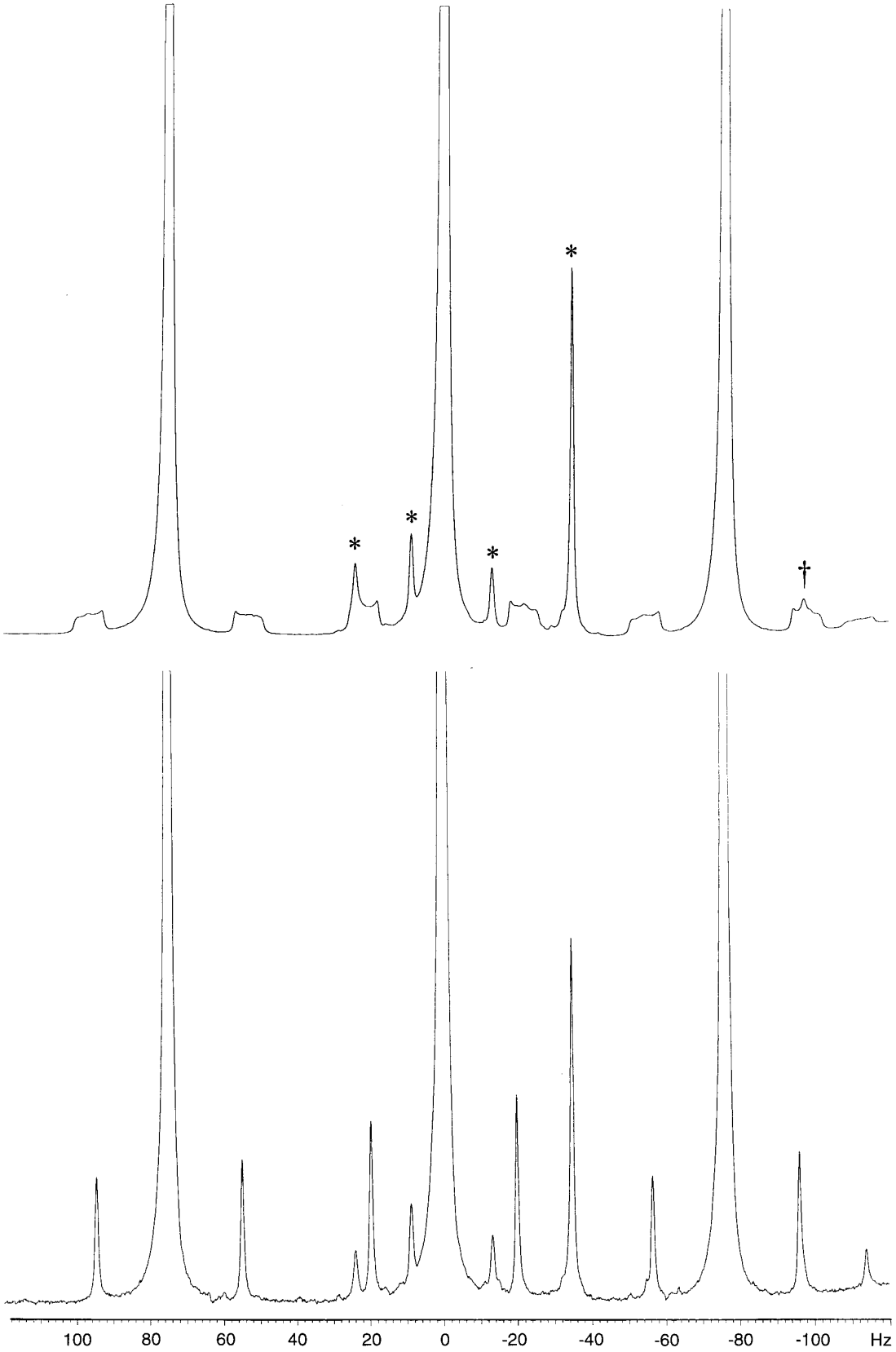


**FIG. 4.** The lower trace is the same as that presented in the top of Fig. 1. The upper trace is the same triplet with the spinning speed variation turned on (416 scans averaged). The asterisks (*) and dagger (†) indicate minor impurity resonances.

VI was created to monitor and store the mass flow controller readout (liters per minute) and the output of the spinner tachometer (hertz).

Spectra were recorded on a Varian Unity 300 spectrometer equipped with an MHU-463 38 gradient matrix shim system from Resonance Research and a 5-mm inverse detection probe from Nalorac.

## ACKNOWLEDGMENTS

The authors thank Professor Adam Allerhand for stimulating this work and Professor Joeseph Dadok for kindly providing reprints.

## REFERENCES

1. S. L. Patt, *J. Magn. Reson.* **96,** 94 (1992).
2. M. Piotto, V. Saudek, and V. Sklenář, *J. Biomol. NMR* **2,** 661 (1992).
3. R. J. Ogg, P. B. Kingsley, and J. S. Taylor, *J. Magn. Reson. B* **104,** 1 (1994).
4. S. H. Smallcombe, S. L. Patt, and P. A. Keifer, *J. Magn. Reson. A* **117,** 295 (1995).
5. G. A. Williams and H. S. Gutowsky, *Phys. Rev.* **104,** 278 (1956).
6. J. Dadok, Twelfth Experimental NMR Conference, Gainesville, FL, February 1971.
7. S. R. Maple, Doctoral dissertation, Indiana University, 1989.
8. B. Bammel and R. E. Avilia, *Anal. Chem.* **52,** 1999 (1980).